Computational and Structural Biotechnology Journal 28 (2025) 211–216

Contents lists available at ScienceDirect

Computational and Structural Biotechnology Journal

journal homepage: www.elsevier.com/locate/csbj

Short Communication

Trajectory generation for ROI expansion in dental CBCT imaging: An out-of-FOV ROI annotation guided arc scan-based approach

S M Ragib Shahriar Islam [a,b,c,*], Ander Biguri [d], Claudio Landi [e], Giovanni Di Domenico [f], Pascal Grün [g], Cristina Sarti [e], Carola-Bibiane Schönlieb [d], Dritan Turhani [g], Gernot Kronreif [a], Wolfgang Birkfellner [b], Sepideh Hatamikia [c,a,b]

[a] Austrian Center for Medical Innovation and Technology, Wiener Neustadt, Austria
[b] Center for Medical Physics and Biomedical Engineering, Medical University Vienna, Vienna, Austria
[c] Clinical AI-Research in Omics and Medical Data Science (CAROM) Group, Department of Medicine, Danube Private University (DPU), Krems, Austria
[d] Department of Applied Mathematics and Theoretical Physics, University of Cambridge, Cambridge, United Kingdom
[e] SeeThrough SrL, Via Bolgara 2, Brusaporto (BG), Italy
[f] Department of Physics and Earth Science, University of Ferrara, Ferrara, Italy
[g] Center for Oral and Maxillofacial Surgery, Department of Dentistry, Faculty of Medicine and Dentistry, Danube Private University (DPU), Krems, Austria

ARTICLE INFO

Keywords:
Dental CBCT
Image reconstruction
Field of view
Trajectory optimization
Interventional radiology
Dose reduction

ABSTRACT

This study introduces a novel optimization approach for source-detector trajectories, designed to simultaneously extend the small dental CBCT field of view (FOV) at specific regions of interest (ROIs) while reducing radiation dose. The proposed algorithm automatically customizes and produces a mechanically feasible arc-based scan trajectory to target predefined ROIs, expanding the FOV beyond the standard range while utilizing only the necessary projections to reconstruct the region of interest, rather than those required for reconstruction of the entire volume. This approach enables a significant reduction in the number of projections. Both qualitative and quantitative analyses, including peak signal-to-noise ratio (PSNR) values greater than 30 dB and structural similarity index measure (SSIM) scores above 0.9, demonstrate that the method successfully enhances the FOV while maintaining high image quality. Notably, the approach achieves a significant reduction in the number of projections up to 47% compared to the conventional limited-angle circular trajectory. This is the first study to explore the simultaneous extension of the FOV and radiation dose reduction in dental CBCT imaging, providing a promising solution for improving clinical outcomes and treatment planning in next-generation CBCT systems.

1. Introduction

The small dental Cone Beam Computed Tomography (CBCT) unit is a specialized X-ray device increasingly used in dental offices for high-resolution 3D imaging of teeth, soft tissues, bones, and nerve pathways in a single scan. However, its primary limitation is its small field of view (FOV). While this can be addressed by using a larger detector, shifted detector scans, or stitching multiple scans, these approaches come with drawbacks such as increased costs, hardware modifications, or additional radiation exposure for patients, making them less than optimal solutions for extending the FOV [1–5].

As an alternative, our previous study [6] was the first to propose an innovative approach that optimizes the source-detector trajectory algorithmically, combined with iterative reconstruction techniques, to effectively expand the FOV without these limitations.

In our previous work [6], we introduced a novel approach to extending the FOV in small dental CBCT units by combining a fusion trajectory with iterative reconstruction algorithms. This method demonstrated its potential to significantly expand the FOV by employing a generic trajectory involving two gantry rotations, effectively acquiring sufficient projection data to reconstruct a much larger 3D volume.

While promising for FOV extension, the proposed trajectory utilized nearly the same number of projections as a conventional limited-angle circular scan. In radiology, however, reducing radiation exposure while maintaining optimal image quality is a top priority [7,8]. Therefore, reducing CBCT imaging dosage is crucial for ensuring safer diagnostics and

* Corresponding author.
E-mail addresses: ragib.shahriar@acmit.at, tusharragib@gmail.com (S.M.R.S. Islam).

https://doi.org/10.1016/j.csbj.2025.06.013
Received 31 March 2025; Received in revised form 3 June 2025; Accepted 4 June 2025
Available online 9 June 2025

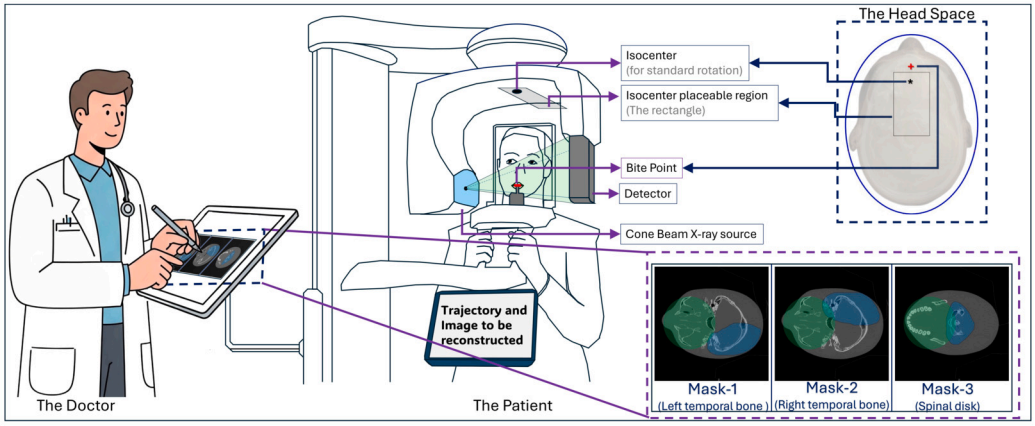

Fig. 1. The imaging setup and the experimental preset masks (blue shades). The green shades indicate the standard FOV.

treatment planning. This consideration prompted us to explore whether our proposed FOV extension could be achieved while simultaneously lowering radiation dose.

Previous research has explored task-driven trajectory optimization to enhance visualization and reduce radiation exposure [9,10]. Additionally, task-dependent studies on CT image reconstruction have focused on dose control and texture management [11].

While these previous studies have made promising advancements in dose reduction using task-specific trajectories, they have not simultaneously addressed FOV extension.

Building on our prior work, which introduced a generic trajectory for FOV expansion [6], and leveraging findings from previous studies that employed task-specific trajectories for dose reduction [9–11], we hypothesize that customizing the trajectory design from our previous research to target specific ROIs, particularly those areas outside the standard dental CBCT FOV, can potentially optimize and reduce the projection selection. By retaining only the most informative projections for reconstructing the region of interest (ROI)—rather than the entire volume—this study proposes the potential to both extend the FOV and reduce radiation exposure by minimizing the required number of projections.

To date, no research has specifically explored optimal customized source-detector trajectories for reconstructing ROIs beyond the standard CBCT FOV. Furthermore, the simultaneous extension of the FOV and reduction of radiation dose is a novel aspect that has not been investigated before and is examined for the first time in this study.

2. Methodology

This study employs the same geometric CBCT dental device simulation model as our previous work [6] which has the capacity of moving isocenter in a 11×6 cm rectangular region. The generalized geometrical setup of the device is shown in Fig. 1. Here, we introduce novel, customized source-detector trajectories designed based on predefined regions of interest (ROIs) specified by the user. For instance, when a dentist identifies an area of interest-particularly those outside the standard small dental CBCT FOV. The study is based on Tuy's conditions [12] for acquiring adequate projection data. Details of the experimental target ROIs are delineated in Section 2.1, while the trajectory development process, adhering to Tuy's conditions, is described in Section 2.2. Finally, the image reconstruction process is explained in Section 2.3.

2.1. Target ROIs

This study explores a method where clinicians specify a desired region outside the standard scan area before imaging. Based on this specified area, we then develop a tailored scan path that expands the FOV in that direction, while keeping the number of scans the same, or ideally, even reducing them.

In our earlier work [6], we reconstructed five areas of interest: the maxillary sinus, the temporomandibular joint (TMJ) bones, the upper and lower jaws, and the chin. For this study, we created three specific masks to target particular areas within these regions on the standard head-sized phantom.

Fig. 1 shows these masks, numbered 1, 2, and 3, which are designed to improve the field of view for the left temporal bone, right temporal bone, and spinal disc area, respectively.

2.2. Trajectory development

For the mechanical feasibility, a continuous and smooth movement path is necessary. In our previous study [6], we determined the search space for the detector's movement, defining the region where the detector can operate without mechanical constraints. Subsequently, we developed an algorithm that produces a large set of geometric position that maximize the addition of information in Tuy's sense. Furthermore, this selection was optimized manually to compensate for missing data, extend the FOV, and ensure that the resulting trajectory remains largely mechanically feasible. In the present study, we have enhanced the geometric position prediction algorithm (Algorithm 1) and integrated it with an additional algorithm (Algorithm 2) to generate mechanically feasible static or dynamic isocentric arc trajectories automatically from the defined mask.

Algorithm 1 The algorithm for finding the heat map from the preset mask.

Data: $Search\ space = \{(i, \Phi_i)\}$; $Presetmask = \{(p, \beta)\}$
Result: $Predicted\ detector\ locations\ and\ angles = \{p', \beta'\}$
for all p from $first$ to end **do**
  if p is outside of region I **then**
    find a pseudo point p' in I;
  else
    if p is near the boundary line **then**
      find pseudo p' in the boundary line;
    else
      $p' = p$;
    end if
  end if
end for
for all β from $first$ to end **do**
  if $\beta \in \Phi_{k_i}$ **then**
    $\beta' = \beta$;
  else
    find the closest β' to β in Φ_{k_i};
  end if
end for

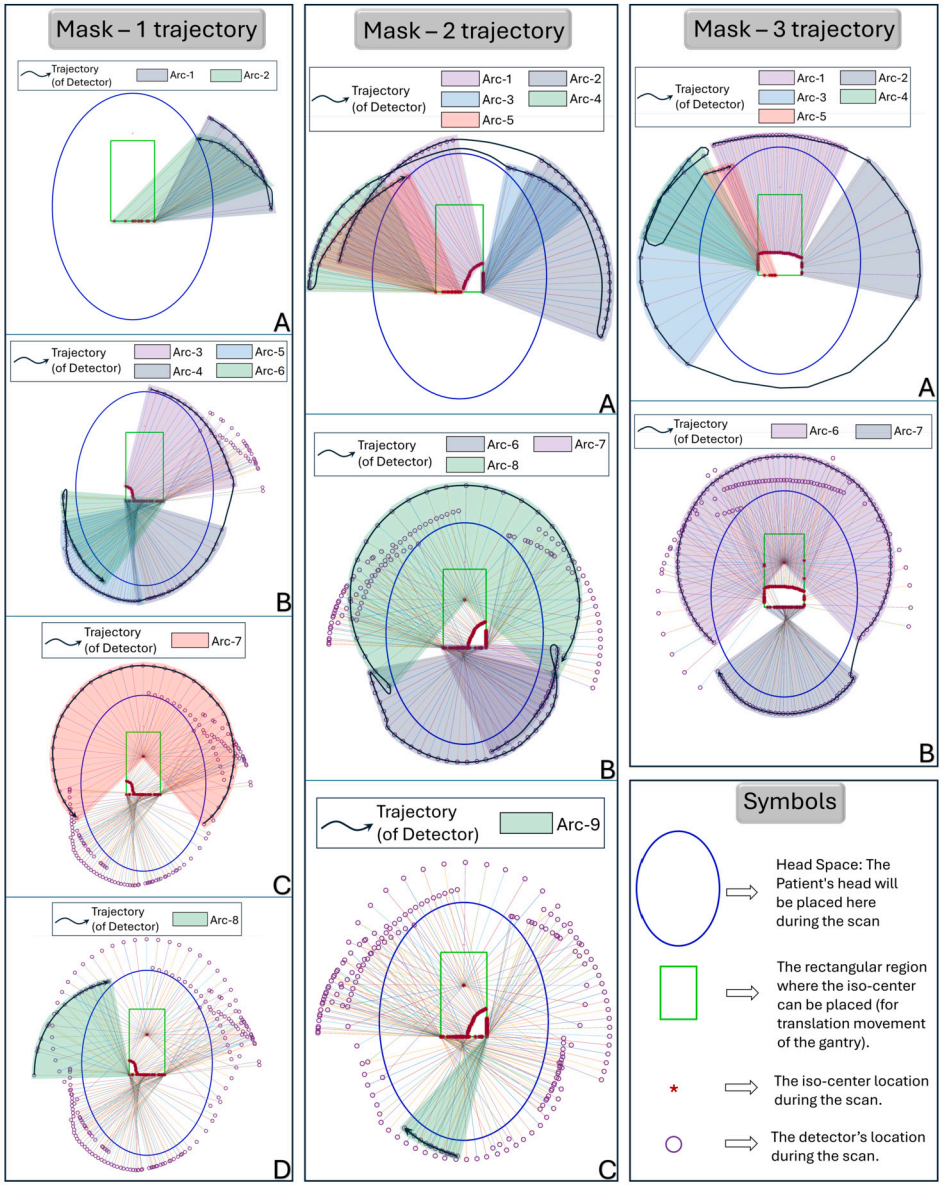

Fig. 2. Trajectories derived from masks 1, 2, and 3. Each colored region represents the area covered by the corresponding arc, while the alphabetic sequence indicates the proposed movement.

Given the coordinates of each isocenter $I = (x, y)$, the isocenter movable region can be described as $I = \{I_1, I_2, ..., I_m\}$. Therefore, the Tuy condition-based calculated search space can be defined as

$$\{(i, \Phi_i) \mid i \in I, \Phi_i = \{\theta_1, \theta_2, ..., \theta_{k_i}\}, \theta_j \in [a_i, b_i] \quad for \quad all \quad j = 1, 2, ..., k_i\}$$

Here, $i \in I$; Φ_i is a set of k_i angles for each i; and each angle θ_j is within the interval $[a_i, b_i]$, where a_i and b_i can vary depending on i. The details about the search space are available at Appendix B.

Moreover, based on Tuy's condition (the details on Tuy's condition and corresponding Tuy's projection angle α_{Tuy} are described in the Appendix A), the preset mask from the clinician can be expressed as follows,

$$\{(p, \beta) \mid p \in \mathbb{R}^2, 0 \leq \beta \leq 2\pi\}$$

And, the predicted detector geometric location with projection angle set can be described as, $\{(p', \beta') \mid p' \in I, \beta' \in \Phi_i\}$

After finding the set of predicted detector positions and the projection angles from Algorithm 1, the trajectory arcs were calculated following the best possible Tuy's condition angle α_{Tuy} (Figure A.1 from Appendix A) to maximize the reconstruction fidelity. Therefore, the trajectory arcs can be described as,

$$\{(r, \alpha) \mid r \in I, \alpha \in \Phi_i\}$$

However, for simplicity, cornered isocenters, boundary line isocenters, and the polyline isocenters are denoted as r_c, r_b, and r_p, respectively in the algorithm.

Later, these arcs were supplemented with a limited-angle circular scan arc to complete the final trajectory. Fig. 2 illustrates the trajectories developed based on our proposed customized trajectory design for the predefined masks 1, 2, and 3, respectively (the masks shown in Fig. 1). These trajectories require a total of 8, 9, and 7 arcs, which could be executed in 4, 3, and 2 continuous movements respectively, to extend the FOV in the targeted regions. A hypothetical chronological sequence of arcs is proposed to complete each trajectory. In total of 204, 220, and 205 numbers of projections were required to reconstruct optimal quality images with the trajectory 1, 2, and 3 respectively.

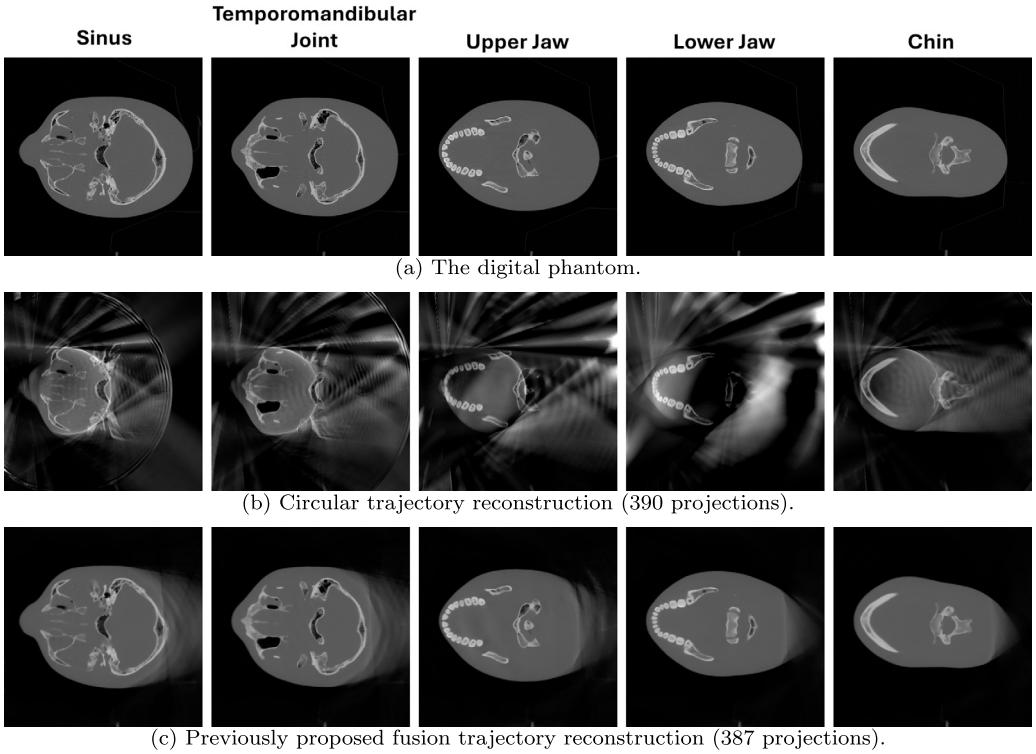

(a) The digital phantom.

(b) Circular trajectory reconstruction (390 projections).

(c) Previously proposed fusion trajectory reconstruction (387 projections).

Fig. 3. Image comparison: phantom, standard, and fusion trajectory.

Algorithm 2 The algorithm for finding the trajectory arcs from the heat map.

Data: $Search\ space = \{(i, \Phi_i)\}$; $Predicted\ detector\ locations\ and\ angles = \{(p', \beta')\}$
Result: $Trajectory\ arcs = \{r, \alpha\}$
  for all p' from $first$ to end **do**
    if p' is a corner point **then**
      $r_c = p'$;
      $\alpha_c = \beta'$;
      reorder α_c to make the arc;
    else
      if r' is on boundary line **then**
        $r_b = p'$;
        $\alpha_b = \beta'$;
        reorder α_b to make path on boundary line for iso-center movement;
        reassign α_b to cover the similar region;
      else
        $r_p = p'$;
        $\alpha_p = \beta'$;
        reorder α_p to make poly-line path for iso-center movement;
        reassign α_p to cover the similar region;
      end if
    end if
  end for

2.3. Image reconstruction

In this study, image reconstruction was performed using the Matlab-GPU-based TIGRE toolbox [13] to facilitate direct comparison with the results of our previous work [6]. Specifically, the ASD-POCS (Adaptive Steepest Descent - Projection Onto Convex Sets) algorithm from the TIGRE toolbox was employed due to its demonstrated high performance to reconstruct 3D volumes from the simulated projections generated by the designed trajectories described in Section 2.2. It is important to optimize the ASD-POCS parameters for every trajectory for better convergence of the algorithm. For this study, an empirical brute-force approach is applied to choose optimal parameter settings. Table 1 shows the important parameter set used for the study. A comparison with reconstruction results from the conventional limited angle circular trajectory was also performed.

Table 1
ASD-POCS parameters for different preset masks.

Parameters	Optimized values		
	Mask 1	Mask 2	Mask 3
niter	15	15	17
lambda	0.1	0.1	0.1
lambda_red	0.9999	0.9999	0.9999
Tviter	50	50	60
maxL2err	90%	90%	90%
alpha	0.002	0.002	0.002
Ratio	0.94	0.94	0.94

3. Results

3.1. Reconstructed images from the developed trajectories

Fig. 3 illustrates the digital phantom and the reconstructed images from the standard circular, and previously proposed fusion trajectory. In comparison, Fig. 4 represents the reconstructed images obtained from the simulated projections of the three mask/region-based trajectories 1, 2, and 3, respectively. In addition, a comparison with reconstruction images from limited circular trajectory (390 projection) as well as proposed generic fusion trajectory from our previous study [6] (387 projections) is performed. This figure highlights the performance of the trajectories in imaging the target regions within the specified slices, as well as their impact on other slices.

3.2. Quantitative analysis

Image quality quantification was performed on the reconstructed limited-angle circular scan and the combined regions of three differ-

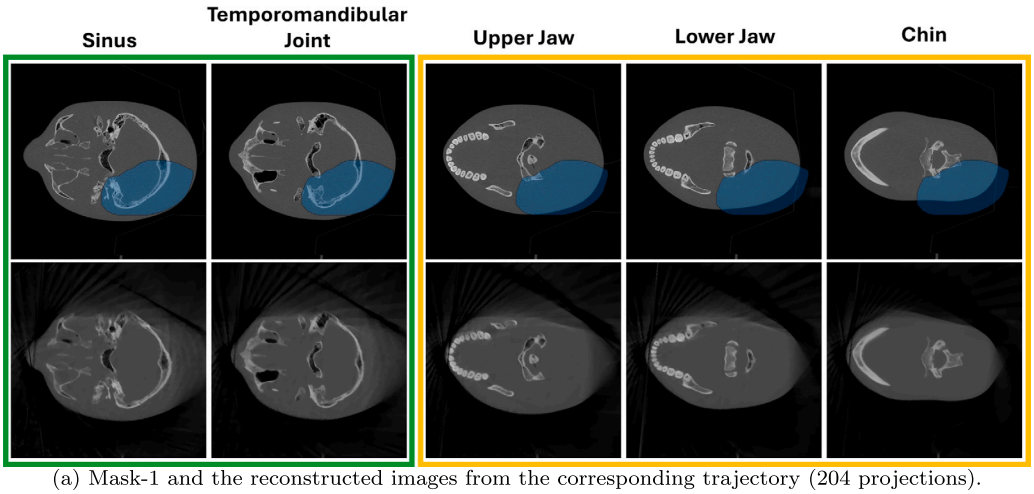

(a) Mask-1 and the reconstructed images from the corresponding trajectory (204 projections).

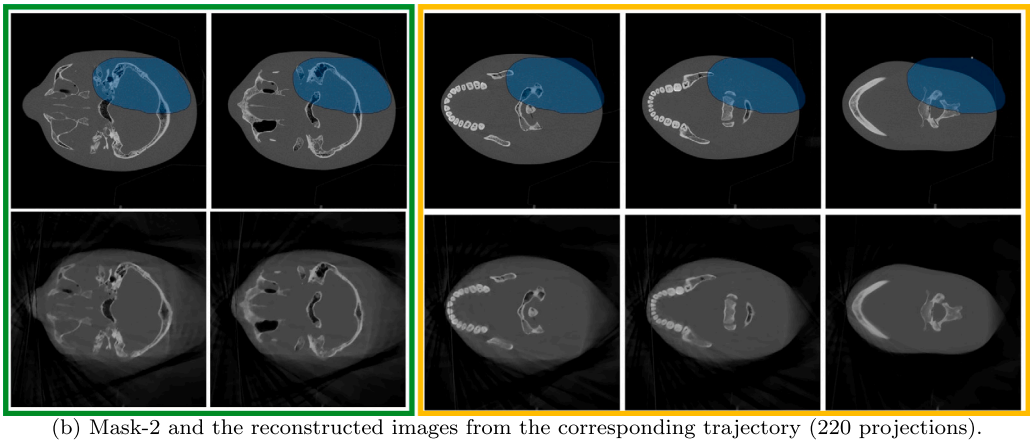

(b) Mask-2 and the reconstructed images from the corresponding trajectory (220 projections).

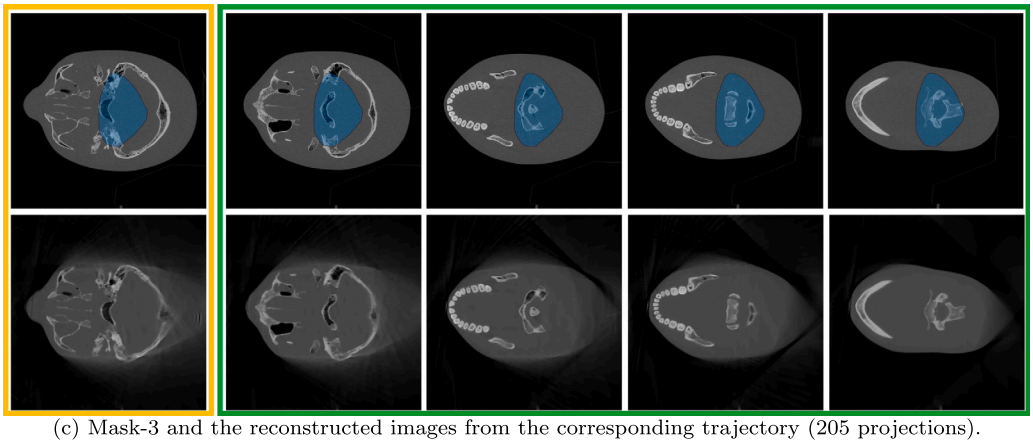

(c) Mask-3 and the reconstructed images from the corresponding trajectory (205 projections).

Fig. 4. Reconstructed images from preset mask-based trajectories in focused (green) and non-focused (yellow) regions.

ent masks. Table 2 presents the quantitative analysis scores for the reconstructed images (Fig. 4) corresponding to Trajectories 1, 2, and 3, respectively. For consistency in comparison, PSNR and SSIM scores were used, and the percentage reduction in scores was calculated relative to the fusion trajectory. The reconstructed images demonstrate excellent performance with the ASD-POCS algorithm. The PSNR (>30 dB) and SSIM (>0.90) scores confirm that the signal-to-noise ratio and reconstruction quality are well within the acceptable range.

4. Discussion and conclusion

This study aimed, for the first time, to expand the FOV in specific predefined ROIs beyond the standard small dental CBCT unit FOV while simultaneously reducing the number of projections—and consequently, reducing the patient's radiation dose. The reconstructed images demonstrate excellent performance, showcasing the effectiveness of the developed customized trajectories. Although a slight decrease in quality metrics is observed compared to the fusion trajectory [6], the trade-off is minimal. Notably, while the limited angle circular trajectory and fusion trajectory [6] require 390 and 387 projections, respectively, our three proposed trajectories achieve comparable results with only 204, 220, and 205 projections, representing a significant reduction of up to 47%. This illustrates that the quality loss is nearly negligible when considering the substantial reduction in projection numbers. Moreover, a previously developed CUDA-based faster version of the ASD-POCS algorithm [14] can reduce the reconstruction time to improve the clinical usability.

Table 2
Performance comparison of trajectories. The non-focused (from the pre-defined masks) ROI scores are represented as shaded cells.

Trajectory ↓	Sinus		TMJ		Upper Jaw		Lower Jaw		Chin	
	PSNR	SSIM	PSNR	SSIM	PSNR	SSIM	PSNR	SSIM	PSNR	SSIM
Mask-1 based trajectory	32.9140	0.9407	33.7119	0.9448	32.4039	0.9447	33.2853	0.9493	36.0630	0.9597
Fusion trajectory (same region)	32.9531	0.9470	33.5116	0.9501	32.9807	0.9479	34.5478	0.9551	36.9741	0.9630
Reduction factor (%)	0.12%	0.67%	-0.60%	0.56%	1.75%	0.34%	3.65%	0.61%	2.46%	0.34%
Mask-2 based trajectory	32.7454	0.9390	33.6810	0.9446	32.8018	0.9454	32.8125	0.9454	35.8110	0.9589
Fusion trajectory (same region)	33.1176	0.9465	33.3876	0.9499	32.4645	0.9418	34.5080	0.9541	37.7890	0.9660
Reduction factor (%)	1.12%	0.79%	-0.88%	0.56%	-1.04%	-0.39%	4.91%	0.91%	5.23%	0.73%
Mask-3 based trajectory	31.7430	0.9528	32.4257	0.9570	31.2189	0.9572	31.3611	0.9605	32.8982	0.9685
Fusion trajectory (same region)	35.8366	0.9573	37.0779	0.9610	35.5836	0.9633	36.3483	0.9674	38.8097	0.9726
Reduction factor (%)	11.42%	0.46%	12.55%	0.42%	12.27%	0.63%	13.72%	0.72%	15.23%	0.42%

Another key aspect of this study is that, although the geometric setup and device modeling from our previous work were used [6], the technical algorithmic development is specifically tailored for next-generation small CBCT dental scanning units. These future CBCT systems will offer greater freedom of movement and fewer mechanical constraints, allowing for the implementation of more versatile source-detector trajectories, such as those proposed in this study. This advancement will enhance dental treatment applications by enabling FOV extension and reducing radiation dose.

CRediT authorship contribution statement

S M Ragib Shahriar Islam: Writing – review & editing, Writing – original draft, Visualization, Validation, Methodology, Investigation, Formal analysis, Data curation, Conceptualization. **Ander Biguri:** Writing – review & editing, Validation, Supervision, Software, Methodology, Investigation, Formal analysis, Conceptualization. **Claudio Landi:** Resources, Project administration, Funding acquisition. **Giovanni Di Domenico:** Writing – review & editing, Supervision. **Pascal Grün:** Validation, Supervision. **Cristina Sarti:** Writing – review & editing, Resources, Investigation. **Carola-Bibiane Schönlieb:** Writing – review & editing, Validation. **Dritan Turhani:** Validation, Supervision. **Gernot Kronreif:** Supervision, Resources, Project administration, Funding acquisition. **Wolfgang Birkfellner:** Writing – review & editing, Supervision, Conceptualization. **Sepideh Hatamikia:** Writing – review & editing, Writing – original draft, Supervision, Project administration, Methodology, Investigation, Funding acquisition, Formal analysis, Conceptualization.

Declaration of competing interest

The authors have declared no conflict of interest.

Acknowledgements

This study was supported by the NÖ FTI Grundlagenforschung project (GLF 21-1-001). In addition, this work has been supported by FFG Project 879733 and ACMIT which is funded within the scope of the COMET program and funded by Austrian BMVIT and BMWFW.

Appendix A. Supplementary material

Supplementary material related to this article can be found online at https://doi.org/10.1016/j.csbj.2025.06.013.

References

[1] Reynolds T, Ma YQ, Kanawati AJ, Constantinidis A, Williams Z, Gang G, et al. Extended intraoperative longitudinal 3-dimensional cone beam computed tomography imaging with a continuous multi-turn reverse helical scan. Invest Radiol 2022;57(11):764–72.
[2] Yang D, Li HH, Goddu SM, Tan J. CBCT volumetric coverage extension using a pair of complementary circular scans with complementary kV detector lateral and longitudinal offsets. Phys Med Biol 2014;59(21):6327.
[3] Stromer D, Kugler P, Bauer S, Lauritsch G, Maier A. Data completeness estimation for 3d c-arm scans with rotated detector to enlarge the lateral field-of-view. In: Bildverarbeitung für die Medizin 2016: Algorithmen–Systeme–Anwendungen. Springer; 2016. p. 164–9.
[4] Gang GJ, Zbijewski W, Mahesh M, Thawait G, Packard N, Yorkston J, et al. Image quality and dose for a multisource cone-beam CT extremity scanner. Med Phys 2018;45(1):144–55.
[5] Hatamikia S, Biguri A, Herl G, Kronreif G, Reynolds T, Kettenbach J, et al. Source-detector trajectory optimization in cone-beam computed tomography: a comprehensive review on today's state-of-the-art. Phys Med Biol 2022;67(16):16TR03.
[6] Islam SMRS, Biguri A, Landi C, Di Domenico G, Schneider B, Grün P, et al. Source-detector trajectory optimization for fov extension in dental cbct imaging. Comput Struct Biotechnol J 2024.
[7] Stanley RJ. Inherent dangers in radiologic screening. Am J Roentgenol 2001;177(5):989–92.
[8] Hatamikia S, Biguri A, Kronreif G, Russ T, Kettenbach J, Birkfellner W. Source-detector trajectory optimization for cbct metal artifact reduction based on piccs reconstruction. Z. Med. Phys. 2024;34(4):565–79.
[9] Capostagno S, Stayman JW, Jacobson M, Ehtiati T, Weiss CR, Siewerdsen JH. Task-driven source–detector trajectories in cone-beam computed tomography: II. Application to neuroradiology. J Med Imag 2019;6(2):025004.
[10] Hatamikia S, Biguri A, Kronreif G, Kettenbach J, Russ T, Furtado H, et al. Optimization for customized trajectories in cone beam computed tomography. Med Phys 2020;47(10):4786–99.
[11] Gao Y, Liang Z, Zhang H, Yang J, Ferretti J, Bilfinger T, et al. A task-dependent investigation on dose and texture in ct image reconstruction. IEEE Trans Radiat Plasma Med Sci 2019;4(4):441–9.
[12] Tuy HK. An inversion formula for cone-beam reconstruction. SIAM J Appl Math 1983;43(3):546–52.
[13] Biguri A, Dosanjh M, Hancock S, Soleimani M. TIGRE: a MATLAB-GPU toolbox for CBCT image reconstruction. Biomed. Phys. Eng. Express 2016;2(5):055010.
[14] Hatamikia S, Biguri A, Kronreif G, Figl M, Russ T, Kettenbach J, et al. Toward on-the-fly trajectory optimization for c-arm cbct under strong kinematic constraints. PLoS ONE 2021;16(2):e0245508.